Submitted to Journal of Composite Materials

THE INFLUENCE OF INTERNAL STRESSES ON THE MICROBOND TEST II: PHYSICAL AGING AND ADHESION

D.-A. Mendels[1], Y. Leterrier, J.-A. E. Månson[2]

Laboratoire de Technologie des Composites et Polymères (LTC)
Ecole Polytechnique Fédérale de Lausanne (EPFL)
CH-1015 Lausanne, Switzerland

and

J. A. Nairn

Materials Science and Engineering
University of Utah
Salt Lake City, UT 84112, USA

ABSTRACT

The present work investigated the effects of physical aging on interfacial adhesion and internal stresses using single-fibre model composites. First, the stress state of the interface and its evolution upon aging were studied for the microbond geometry. This stress analysis was used with experiments to determine an intrinsic interfacial shear strength. Second, this stress analysis, including aging effects, was used in a fracture mechanics or energy release rate analysis of the microbond test, which involves the energy necessary to propagate a crack instead of the minimum stress to initiate a crack. These methods were tested for both freshly cured and aged epoxy droplets on glass fibres, and were shown to yield similar results. It was found that neither the interfacial shear strength nor the interfacial toughness were changed by physical aging of the polymer matrix when the relaxation of internal stresses and shift of relaxation times of the matrix due to physical aging were accounted for. Thus, the intrinsic shear strength and toughness of the fibre/matrix interface were determined.

---

[1] Present address: National Physical Laboratory, Teddington, Middlesex, TW11 0LW United Kingdom

[2] to whom correspondence should be addressed

KEYWORDS: Microbond test, adhesion, intrinsic strength, internal stresses, physical aging, energy release rate, interfacial toughness

1 INTRODUCTION

The durability of composite materials is the result of complex interactions between the reinforcing fibre, the polymer matrix and the fibre/matrix interface [1, 2]. The homogeneous stress state often found in a neat polymer is radically modified in a composite by the internal stress state of the matrix, as well as by additional stress resulting from loading of the composite structure [3]. Internal stresses in a composite are caused by differential curing and/or thermal shrinkage between the matrix and the fibres during fabrication of the composite. Additionally, when a polymer matrix is cooled below its glass transition temperature, T_g, it departs from thermodynamic equilibrium. The subsequent slow evolution of the polymer towards equilibrium, termed structural recovery, significantly affects its mechanical properties, by a process known as physical aging [4]. Changes in viscoelastic properties of the composite during physical aging have been studied, for instance using classical laminate theory [5, 6] or the finite element method (FEM) [7-10].

The influence of local stress concentrations at the fibre/matrix interface on the structural recovery and aging of the polymer has not been clearly established, although structural recovery is known to profoundly change the viscoelastic response of a polymer [11]. Such a phenomenon complicates analysis of the failure of composites, which is controlled to a large extent by the interfacial strength.

The present work investigated how interfacial properties are modified as a result of physical aging. First, the stress state of the interface and its evolution upon aging were studied for the microbond geometry. This stress analysis was used with experiments to determine an intrinsic interfacial shear strength. Second, this stress analysis, including aging effects, was used in a fracture mechanics or energy release rate analysis of the microbond test. Provided that all internal stresses and aging effects in internal stresses were properly included, both the

strength analysis and the energy analysis led to the same conclusion --- the interfacial failure properties were not affected by aging. A condensed version of this article was presented at the Duracosys'99 conference [12].

2 THEORY

2.1 *Modelling of interfacial shear strength for the microbond test*

The microbond test has been extensively used to assess the shear strength of polymer/fibre interfaces [13]. In this test, the interfacial shear strength is determined from the force required to debond a droplet of cured resin on an individual fibre. Analysis of microbond test results requires precise measurement of the dimensions of the droplet (L and r_d or length and radius), together with the fibre radius (r_f). The apparent contact angle of the solid droplets and the volume and radius of a cylinder that is equivalent in volume and of same length as the droplets - referred to as the equivalent cylinder in the following - are subsequently determined using the Carroll equation [14], which describes a liquid droplet profile (i.e., it is assumed that the unduloid shape of the initial liquid droplet remains unduloid after solidification). Microbond tests were conducted and their validity checked, according to the procedures described later in the experimental section. The recorded load at debonding, $F_{\max}$, was obtained, as well as the frictional force after debonding, F_{fric}, as shown on a typical force vs. displacement graph in Figure 1.

The experimental shear stress in a microbond test, which is simply the average shear stress on the interface, can be determined from the force at debond F_{max} using:

$$\tau_{exp} = \frac{F_{\max}}{2\pi r_f L} \tag{1}$$

In a recent paper, this classical interpretation of the microbond test was modified using a novel elastic stress transfer model [15], following two different approaches: either by introducing the exact droplet profile into the analysis, or by using an equivalent cylinder method [16]. The former requires numerical integration, whereas the equivalent cylinder model results in an analytical formulation. These two approaches were shown to be equivalent and result in the determination of the same interfacial shear stress.

It was shown in Ref. [16] that the interfacial shear stress varies along the interface and results from two distinct contributions, namely the applied force (F_{max} or τ_{exp}) and the internal stresses. Some typical shear-stress profiles are reproduced in Figure 2. When using exact droplet profiles, the peak shear stress occurs at the inflection point of the droplet, which is very near the end of the droplet. In equivalent-cylinder model, the peak shear stress occurs at the ends (see Figure 2) and is essentially equal to the peak shear stress in the full droplet profile analysis. Instead of assuming that microbond specimen failure is controlled by the average shear stress (τ_{exp}), the strength model in Ref. [16] assumed that failure occurs when the peak shear stress equals the intrinsic shear strength or τ_0. By equating the peak interfacial shear stress under load F_{max} to the intrinsic shear strength using the equivalent-cylinder model, the experimental shear stress can be derived as an analytical expression in terms of the intrinsic shear strength and a contribution due to internal stresses (the K term):

$$\tau_{exp} = \tau_0 \frac{\tanh \beta L}{\beta L} + K \frac{\tanh \beta L/2 \tanh \beta L}{\beta L} \tag{2}$$

The parameter β was determined from the elastic and geometric properties of the system (fibre and matrix moduli E_f and E_m, and radii, r_f and r_d, and matrix Poisson's ratio ν_m) and from its geometry [15]:

$$\beta = \left[\kappa \frac{r_f^2 E_f + \left(r_d^2 - r_f^2\right) E_m}{r_f E_f \left(1 + \nu_m\right)} \right]^{1/2} \tag{3}$$

where κ is a structural parameter given by:

$$\kappa = \frac{12.\left(2\left(r_d - r_f\right) + \xi\left(r_d^{\,2} - r_f^{\,2}\right)\right)}{r_f\left\{24r_f\left(r_d^{\,2} - r_f^{\,2}\right) - 16\left(r_d^{\,3} - r_f^{\,3}\right) - 3\xi\left(r_f^{\,2} - r_d^{\,2}\right)^2 + 6r_d\left(2 + \xi r_d\right)\left[2r_d^{\,2}\ln\left(r_d \big/ r_f\right) - \left(r_d^{\,2} - r_f^{\,2}\right)\right]\right\}} \tag{4}$$

where $\xi = -E_m / r_f E_f$ was determined semi-empirically in ref. [15], and recently received experimental validation [17].

The micro-mechanical study was completed by the determination of the internal stress factor *K*, as described in the following section. Rather than using the simple formulation of a thermo-elastic stress state, the analysis accounts for time/temperature/aging-time effects. By properly including all internal stress effects through changes in *K*, Equation (2) can be used to determine whether observed changes in τ_{exp} following aging are due to changes in the intrinsic shear strength of the interface, or due to changes in the internal stresses, or due to a combination of the two.

2.2 *Internal stresses and their evolution upon aging*

This section establishes the basis for modelling the relaxation of process-induced internal stresses near the interface. Internal stresses build up during processing of thermoset systems as a result of [18]:

- chemical shrinkage of the resin during curing: the composite with resin in a liquid state is brought to an elevated temperature, above or below the resin infinite T_g, which, while curing, builds up stiffness and shrinks at the same time. In the present work, the cure of the resin took place far above the ultimate T_g of the resin (cure at 100°C, T_g = 42.1°C) and over 24 hours. The resulting Young's modulus of the resin is small at the cure temperature, as well as the relaxation time. As a result, chemically induced internal stresses are negligible for this particular system and geometry: this assumption is well supported by

experimental internal stress measurements carried-out in Ref. [18] on systems with similar chemistry;

- thermal shrinkage during cool-down from the cure temperature to ambient or an aging temperature, since the resin and its reinforcement usually do not have the same coefficients of thermal expansion. In the present work, the cool-down from the cure temperature to T_g also involved low Young's modulus of the matrix and short relaxation times. Taking 100MPa for the matrix Young's modulus above its T_g and a characteristic relaxation time of 1s relaxed thermal stresses were evaluated to be less than 0.5% of the total internal stress calculated following the formalism introduced in section 2.2.4 below. Thus, the evolution of internal stresses above the glass transition temperature could be neglected in the present analysis. This situation no longer holds when the polymer is cooled-down below its T_g.

Depending upon the resin behaviour, the following evaluations of the internal stress parameter are possible.

2.2.1 *Elastic stress*

As a first approximation, K can be derived from a temperature-independent, thermoelastic stress analysis [19]:

$$K_0 = r_f \beta E_f \left(\alpha_g - \alpha_f\right) \frac{\Delta T}{2} \tag{5}$$

where α_f and α_g are the coefficients of thermal expansion of respectively the fibre and matrix below its T_g and ΔT is T- T_g. This simple case has been widely used in the literature, although it clearly corresponds to a upper bound to the real internal stress level. Equation (5) assumes that the Young's moduli of the resin and fibre, and their coefficients of thermal expansion are constant over the temperature range ΔT. As a result, the slope of a K vs. T plot is a constant, as shown in curve 1 of Figure 3. This gross approximation is particularly false close to the

glass transition of the polymer, which generally involves an abrupt change in Young's modulus.

2.2.2 *Thermo-elastic stress*

It is important to note that Equation (5) includes the matrix stiffness through the parameter β. When the matrix stiffness depends on temperature, the evolution of E_m with temperature can be included by integration during cool-down. In most cases, the coefficient of thermal expansion of the resin below its glass transition, α_m, can be considered constant within a few percent error. As such, the internal stress parameter becomes:

$$K_0 = r_f E_f \left(\alpha_m - \alpha_f\right) \frac{\Delta T}{2} \int_{T_g}^{T_{test}} \frac{d\beta}{dT} dT \tag{6}$$

A typical result of this approach is to decrease the slope of the K vs. T plot, as well as the value of K_0, as shown in curve 2 of Figure 3. This approximation is, however, independent of the cooling rate, whereas most polymers are well known to exhibit viscoelastic behaviour under their glass transition, with associated stress relaxation. Relaxation during cool-down, yielding $K_0 = K(t=0)$, as well as at the equilibrium temperature, yielding $K(t)$, must therefore be introduced in Equation (5) in order to more accurately describe the internal stress level.

2.2.3 *Thermo-viscoelastic stress*

A classical mechanical model presented to describe the relaxation behaviour of polymers is based on a parallel combination of Maxwell elements, yielding the elementary relaxation response of an element i [20]:

$$E_i(t) = E_{0i} \exp\left(-t/\lambda_i\right) \tag{7}$$

where E_{0i} is the original modulus at t=0 associated to the i^{th} element and λ_i the characteristic relaxation time for this element. The relaxation modulus is then expressed for a distribution of N relaxation times using:

$$E(t) = \sum_{i=1}^{N} E_{0i} \exp(-t/\lambda_i) \tag{8}$$

When the spectrum of relaxation times is expanded to a continuous distribution $\psi(\lambda)$, the above equation becomes:

$$E(t) = \int_0^{\infty} \Psi(\lambda) \exp(-t/\lambda) d\lambda \tag{9}$$

A useful expression of this integral was derived by Kohlrausch [21], which results in approximating Equation (9) by a stretched exponential law:

$$E(t) = E_0 \exp\left(-(t/\lambda)^w\right) \tag{10}$$

where E_0 is the unrelaxed modulus, λ is the global relaxation time and w is a parameter related to the width of the relaxation time spectrum. This approach was used because of its great simplicity; the total viscoelastic response is described by means of only three parameters, and the approach has been established by several independent workers on microstructural bases [22, 23]. However, as the most general form of the stretched exponential was shown to accurately describe relaxation of amorphous polymers below their T_g [24], the relaxation modulus is expressed as:

$$\frac{E(t) - E_\infty}{E_0 - E_\infty} = \exp\left(-(t/\lambda)^w\right) \tag{11}$$

where E_∞ is the relaxed modulus. The introduction of a relaxed modulus $E_\infty \neq 0$ is needed to describe the relaxation behaviour of most amorphous polymers which, generally, do not relax down to a zero stress after being submitted to a strain. In the simple case where no structural recovery occurs, the global relaxation time generally follows:

$$\lambda = \lambda_r a_T \tag{12}$$

where a_T is a global temperature shift factor generally determined by the Williams-Landel-Ferry (WLF) law [17].

In this analysis, the internal stress relaxation is assumed to follow a relaxation law similar to that of the relaxation of the matrix Young's modulus:

$$\frac{K(t)-K_\infty}{K_0-K_\infty}=\exp\left(-(t/\lambda)^w\right) \tag{13}$$

From Equations (12) and (13) the slope of the K vs. T plot gradually increases with decreasing temperature below T_g, with a resulting value of K_0 lower than in the former cases, as shown in curve 3 of Figure 3.

2.2.4 *Thermo-viscoelastic including aging stress*

A simple linear viscoelastic law, i.e. an exponential retardation function is not sufficient to describe the salient features of structural recovery [2], and the stress relaxation modulus $E(t)$ of a quenched and annealed amorphous glass changes not only with the load time t but also with the aging time t_e. In this sense, Equation (11) together with (12) are inadequate for describing the stress relaxation in the glassy state, since a structural recovery term δ is required to describe the aging behaviour.

In the present work, a model was chosen to accurately describe the polymer behaviour when it is aged below its glass transition temperature T_g. If one cools an amorphous polymer from above to below T_g, as depicted in Figure 4, and then keeps the temperature fixed, the volume of the material evolves spontaneously towards equilibrium [25]. Such behaviour is also obtained if the enthalpy instead of the volume is measured, so that the evolution of the glassy polymer's thermodynamic state has been termed structural recovery. This change in internal state is characterised by some physical changes, such as the engineering properties of the polymer [26-29]. The sum of these changes has been termed physical aging, to distinguish

it from chemical aging, since all the changes are completely reversible when the polymer is reheated to above its T_g.

A Narayanaswamy-Moynihan [30, 31] formalism was chosen together with a more classical Kohlrausch-Williams-Watts (KWW) [21, 32] stretched exponential function to describe the relaxation tests, and the internal stress parameter K. It was demonstrated in reference [33] that Equation (11) is consistent with the Narayanaswamy-Moynihan development of the KWW form. The Narayanaswamy-Moynihan equation is a general development of the Kovacs, Aklonis, Hutchinson and Ramos model (KAHR model) [34]; the former involves a continuous distribution of relaxation times, while the latter deals with a discrete spectrum of relaxation times. They formally use a multiple ordering parameter model to define the viscoelastic response function for the glass, and describe the volume departure from equilibrium. Following references [30-34], Equation (12) is replaced by:

$$\lambda(T,\delta) = \lambda_r a_T a_\delta \tag{14}$$

to account for structural recovery. The shift factors are defined by:

$$a_T = \lambda(T,0)/\lambda(T_r,0) = \exp[-\Theta(T - T_r)] \tag{15}$$

$$a_\delta = \lambda(T,\delta)/\lambda(T,0) = \exp[-(1-x)\Theta\,\delta/\Delta\alpha] \tag{16}$$

where T_r is a reference temperature, taken as T_g in the present work, and $\delta = 0$ denotes equilibrium. Θ and $0<x<1$ are material parameters, $\Delta\alpha = \alpha_l - \alpha_g$ with α_l and α_g respectively the liquid and glass coefficients of thermal expansion. It is important to note that the whole spectrum of retardation times is shifted along the time axis, i.e. its shape does not change. It thus supposes that w is a constant versus the aging time. Equations (11) and (14) to (16) provide a formalism for the description of the relaxation behaviour of a glass once the functions for the shift factors a_T, a_δ, and the material parameters are known.

A schematic representation of the internal stress parameter in a thermo-viscoelastic analysis including aging effects is presented in curve 4 of Figure 3. One important feature resides in the considerable difference between the thermo-elastic and thermo-viscoelastic approaches to thermal stresses. A thermo-elastic approach provides an upper bound to the internal stress level. Furthermore, large differences appear when the material is held at an aging temperature prior to quench to a test temperature. Due to structural recovery and the associated shift of retardation times, the internal stress level becomes higher than that of the freshly cured resin if the test temperature is far enough from T_{aging} and T_g. In this case, for test temperature $T_{test,1}$, following the internal stress build-up given by curve 4 clearly leads to higher values than would be given by curve 3. On the other hand, at test temperature $T_{test,2}$ the opposite result is found.

2.3 *Energy release rate formulation*

An alternate method for interpretation of microbond tests is to use fracture mechanics or to assume that an interfacial crack propagates when the energy release rate for crack growth, *G(a)*, exceeds a critical value or the interfacial fracture toughness, G_c [35, 36]. Because the energy release rate is a function of crack length, especially when there is friction on the interface (as shown by the friction on the fully debonded interface in Figure 1), this analysis requires experimental observation of the crack length as a function of applied load. Unfortunately, it is very difficult to measure crack growth in microscopic specimens. As an alternative, the analysis in Reference [35] predicts that an interfacial crack should propagate stably along the entire interface and that the peak load ($F_{\max}$) corresponds to an instant in time when the crack length is approximately equal to the droplet length. Based on finite element results, it was further suggested that an acceptable energy release rate for a crack length nearly equal to the droplet length (*G(a)* as *a* approaches *L*) can be acceptably calculated from the energy release rate for a droplet that has a much greater length than the actual droplet but

a crack length of $a = L$: this associate geometry is shown in Figure 5. In other words, the energy release rate at the peak load for a microbond droplet of length L is

$$G_\infty(L) = \lim_{l\to\infty} G(L,l) \tag{17}$$

where $G(L,l)$ is the energy release rate for a droplet of length l ($>L$) with crack of length L. The resulting analytical expression for microbond energy release rate at $F_{\max}$, including effects of interfacial friction and internal stresses, is taken from Ref. [35] and recasted in terms of τ_{exp}, for the purpose of the present analysis:

$$G_\infty(L) = \frac{2C_{33s}L^2}{r_f}\left(\tau_{\exp} - \tau_f\right) + 2LD_{3s}\Delta T\left[\tau_{\exp} - \tau_f\left(1+\frac{1}{2\beta L}\right)\right] + \frac{r_f\Delta T^2}{2}\left(\frac{D_3^2}{C_{33}} + \frac{\upsilon_m(\alpha_T - \alpha_m)}{\upsilon_f A_0}\right) \tag{18}$$

where τ_f is the frictional stress on the interface, α_T and α_m are the coefficients of thermal expansion (CTE) for fibre (transverse) and matrix, and ΔT is an effective temperature differences describing the internal stresses. Here ΔT will be calculated using the various models described in the previous section. The factor β in this analysis is taken from the previous model (Eq. (2) to (4)), and therefore corresponds to the equivalent cylinder stress transfer parameter, υ_m and υ_f are the matrix and fibre volume fractions. The other coefficients are obtained using the following equations, in which subscripts A, T stand for axial and transverse properties of the fibre and subscript m refers to a matrix property:

$$A_0 = \frac{\upsilon_m(1-\nu_T)}{\upsilon_f E_T} + \frac{1-\nu_m}{E_m} + \frac{1+\nu_m}{\upsilon_f E_f} \tag{19}$$

$$A_3 = -\left(\frac{\nu_A}{E_A} + \frac{\upsilon_f\nu_m}{\upsilon_m E_m}\right) \tag{20}$$

$$C_{33} = \frac{1}{2}\left(\frac{1}{E_A} + \frac{\upsilon_f}{\upsilon_m E_m}\right) - \frac{\upsilon_m A_3^2}{\upsilon_f A_0} \tag{21}$$

$$C_{33s} = \frac{1}{2}\left(\frac{1}{E_A} + \frac{\upsilon_f}{\upsilon_m E_m} \right) \tag{22}$$

$$D_3 = -\frac{\upsilon_m A_3}{\upsilon_f A_0}(\alpha_T - \alpha_m) + \frac{1}{2}(\alpha_A - \alpha_m) \tag{23}$$

$$D_{3s} = \frac{1}{2}(\alpha_A - \alpha_m) \tag{24}$$

For an isotropic fibre, such as glass in the present work, α_A and α_T are simply replaced by the fibre's isotropic coefficient of thermal expansion α_f. The frictional stress τ_f is obtained directly from the frictional force measured after failure of the interface from the experimental pull-out curve:

$$\tau_f = \frac{F_{fric}}{2\pi r_f L} \tag{25}$$

3 EXPERIMENTAL PROCEDURE

3.1 ***Thermal history***

The resin employed was a Diglycidyl Ether of Bisphenol A (DGEBA, Dow Chemicals DER332), cured with a diamine (Jeffamine D400) in a stoichiometric amount. The resin was preheated for 3 hours at 60°C to melt any residual crystals. The two constituents were then stirred manually until the solution was clear, and carefully degassed in a vacuum oven at 40°C for 10 min. The cure cycle was chosen as described in Ref. [26], i.e. 24 hours at 100°C and then quench to 50°C, the annealing temperature. The resulting glass transition temperature T_g of 42.1°C was measured by Differential Scanning Calorimetry using a heating rate of 20°C/min, following a cooling of the sample from 100°C to 10°C at 20°C/min.

When non-destructive testing was performed on specimens, e.g. small strain relaxation tests, their thermal history was erased at 50°C for at least 30 minutes. They were subsequently quenched to the aging temperature 37°C (or T_g -5.1°C) and either aged isothermally for a time t_e, as depicted in Figure 6, or cooled directly to the experimental temperature T_{test} = 22°C for the subsequent microbond tests.

In all cases, an unaged state cannot be obtained, because the cooling rate is never fast enough, one therefore always needs to correct for thermal transfer effects. Thermal inertia was accounted for using the approximation introduced by Crissman and Zapas [37]. These authors have demonstrated that, for most glasses and polymers, thermal inertia is accounted for, involving an error of less than 0.1% on the relaxation modulus, by increasing the aging time by t_{cool} / 2, where t_{cool} is the time required to cool the specimen. The values of cooling times were found as defined in Table 1; values for the epoxy rod were obtained experimentally, whereas values for the microbond specimen were calculated. The heat-transfer coefficient for quenching in air by natural convection was determined from the epoxy rod experiment, and the time it takes to cool a microbond specimen, assimilated to a 200 μm diameter sphere of epoxy, was subsequently calculated using Heisler charts [38]. Typical thermal properties of an epoxy were used, the heat capacity being C_p = 1 J/g.K and the thermal conductivity k = 0.2 W/m.K. As presented in Table 1, the time to cool a microbond sample was less than 1s so that it was discarded in the calculations, since it involved a deviation of only 0.5% on the total relaxation time. When the specimen was aged, two cooling time corrections were involved, whereas only one was needed for a quench from 50°C to the experimental temperature. A time t_{test} was required to mount the sample, and accounted for by using Equation (13).

3.2 *Microbond test*

Reproducible droplet sizes were obtained using a fibre that was immersed in the resin and removed at a relatively high speed. The droplets that formed on the fibre were subse-

quently transferred to the experimental fibre by simple contact. A matrix Young's modulus of 1.85 GPa and Poisson's ratio of 0.35 were determined by Electronic Speckle Pattern Interferometry (ESPI) [3, 39] in the strain range 10^{-4} to 10^{-3}. ESPI is a full-field, non-contact, strain measurement technique with a resolution below the micrometer. The experimental set-up used here, and described in Ref. [3], allowed a quasi-simultaneous measurement of displacements in 3 directions (two in-plane, one out-of-plane) after one load step has been applied to a tensile coupon. The displacement map of the tensile coupon was differentiated to obtain the strain map, and the Young's modulus and Poisson's ratio were obtained within a standard deviation of 1% and 9%, respectively.

E-type glass fibres with a diameter of about 11 μm, modulus E_f = 72 GPa, and a γ-APS (OSI Specialties aminosilane 1100) surface treatment, were taken from a woven fabric.

In order to determine the droplet dimensions, the fibres were mounted under zero pretension on lateral supports on a microscope slide. The fibres and droplets were then stuck on a support using cyanoacrylate glue and the assemblage was mounted on a 4 N load cell. Extreme care was used to align the support and fibre perpendicular to the jaws of the microbond device.

The pull-out set-up had Teflon jaws (2.5mm thick) clamped by a pneumatic set-up. The device allowed a negligible friction force on the fibre, while the radial clamp force on the fibre was controlled within 5 kPa. The jaws were mounted on a stable support, and pull-out was induced through vertical displacement of the load cell, mounted on the crosshead of a tensile testing machine set to a speed of 0.5 mm/min.

When a large population of droplets are tested, a scatter as high as 20% of the standard deviation in force at break is usual. In order to limit this scatter, the following criteria were defined from the force versus displacement curves up to debonding [16]. While the ideal force vs. displacement graph would be such as that shown in Figure 1, multiple breaks, anomalies at the initiation of the load, and tests where cohesive rather than adhesive failure had occurred

were discarded from the analysis. Obviously, the tests where the fibre breaks before the interface were also omitted.

3.3 *Cast coupon and relaxation test*

The resin described above was also cast into silicon moulds and cured in an oven using the same conditions. Dog-bone shaped samples were milled from the cast coupons, and tested in small-strain relaxation tests, as described below.

Dynamic viscoelastic analyses over a two-decade frequency range from 1 to 100 rad/s and temperatures from 17°C to 67°C were carried out by means of a Dynamic Mechanical Thermal Analyser RSA II (Rheometrics), in 3-point bending of a 40 X 10 X 2 mm^3 specimen. The specimens, which were previously stored in a desiccator at room temperature, were mounted and heated to 50°C for 5 minutes, and then cooled at 20°C.min^{-1} to the test temperature. The sample was left for 1 minute to equilibrate at the test temperature, with t_{cool} estimated as being 50 s, then tested. Prior to the next test the sample was re-heated and held for 2 min at 50°C to erase its' thermal history and the procedure was repeated. Aging phenomena were thereby minimised and not taken into account in the analysis of dynamic mechanical experiments.

Small-strain relaxation tests were performed at different aging times t_e, according to the following procedure. The specimen was brought to a fixed initial strain, $\varepsilon_0 = 0.01$, with a fast loading rate of 2.10^{-2} s^{-1}. The strain was then maintained at this value by means of a closed loop control system. The stress evolution, $\sigma(t)$, was recorded as a function of time for a relaxation period of 1 hour. Following previous studies, the results presented in Figure 7 were expressed in term of the relaxation modulus $E(t) = \sigma(t) / \varepsilon_0$. In order to increase the resolution for E_0 it was further measured using ESPI in the strain range 10^{-4} to 10^{-3}. Theoretically, true stress-relaxation modulus is obtained when the strain is applied instantaneously, which is not possible practically. Methods to overcome the drawback of finite strain rate have been pro-

posed and they were reviewed by Lin and Aklonis [40]. In this study, the uncertainty of the experimentally measured data was about 1%. Following Smith's approach, the deviation between experimental and true stress-relaxation moduli was reduced to less than 1% after an interval of time equal to 10 times the constant strain rate period [41]. Based on this argument, data collected 5 s after the onset of the measurement, i.e. 10 times the 0.5 s required to achieve the 1% strain, were assumed to accurately represent the true stress-relaxation moduli and were used in the present analysis.

4 RESULTS AND DISCUSSION

4.1 *Viscoelastic behaviour of the matrix subject to physical aging*

The exponent w characterising the width of the spectrum of relaxation times was first determined by the dynamic viscoelastic properties of the epoxy through the glass transition region. In this experiment, the complex tensile modulus E^* was studied. It can be separated into the real and imaginary parts E' and E'':

$$E^*(z) = E'(z) + iE''(z) \tag{26}$$

where z is a non dimensional frequency. Starting from the KWW Equation (11), and using one Fourier transform followed by one Laplace transform, Chow demonstrated that the storage and loss moduli can be calculated from [42]:

$$\frac{E'-E_\infty}{E_0-E_\infty} = 1 + \sum_{m=1}^{\infty} \frac{(-1)^m \Gamma(mw+1)}{m!\, z^{w\lambda}} \cos(mw\pi/2) \tag{27}$$

and

$$\frac{E''-E_\infty}{E_0-E_\infty} = \sum_{m=1}^{\infty} \frac{(-1)^{m+1} \Gamma(mw+1)}{m!\, z^{w\lambda}} \sin(mw\pi/2) \tag{28}$$

The theory and experiment for the epoxy resin are compared in Figure 7. The experimental points in Figure 7 have been shifted horizontally along the time axis to form the 'master curve'. The reference temperature for the master curve is 41.2°C, conventionally taken as the maximum of the peak tan(δ). The full curves present the theoretical calculation where (E_0,E_∞) = (1.85,0.01) GPa and the exponent w equals 0.33.

The relaxation modulus of the epoxy network is shown in Figure 8 as a function of aging time, and described by a KWW type model [27]. This type of representation is used to obtain the time/aging-time shift factor a_δ, as well as the aging rate [4].

This experiment was completed by the determination of the Young's modulus variation with aging time by ESPI, as shown in Figure 9. The horizontal shifts, a_δ, along the time axis were then obtained as:

$$a_\delta = \lambda(t_e)/\lambda(t_e(ref)) \tag{29}$$

where $\lambda(t_e)$ is the value of λ at the relevant aging time and $\lambda(t_e(ref))$ is the λ at the reference aging time, chosen as 7 min, as detailed before. In Table 2, we present the parameters determined for each aging experiment following Equation (11), and the resulting double logarithmic plot of aging time shift factor a_δ versus aging time is shown in Figure 10. The linearity obtained allows the double-logarithmic shift rate μ to be determined as:

$$\mu = d\log(a_\delta)/d\log(t_e) \tag{30}$$

From the present set of experiments the shift rate was determined as $\mu = (7.9\pm0.1)\times10^{-2}$ as in Figure 10.

Table 3 summarises the material parameters determined through this study and from references [26-29]. The parameter $\Delta\alpha$ was obtained from a quasi-linear plot from the dilatometer experiments of Duran and McKenna [43].

It was further found that the exponent w equals 0.33±0.04 from the relaxation tests depicted in Figure 8. It is thereby verified that within experimental error viscoelastic properties of the epoxy studied involve one unique distribution of relaxation times, and the shape of the relaxation time spectrum defined by w does not depend upon the aging time.

4.2 *Effect of aging on the interfacial shear strength*

When the interfacial shear stress τ_{exp} was plotted versus the droplet length, it decreased with increasing specimen size (Fig. 11). There was also a marked increase, close to 40%, in τ_{exp} after aging (Fig. 11). By Equation (2), this increase may be due to an increase in intrinsic shear strength (τ_0) or to a decrease in internal stresses (K). Internal stresses may change due to chemical or physical aging. We ruled out chemical aging effects by reheating a series of aged microbond samples above T_g and doing more microbond tests. Because the results showed similar values of τ_{exp} compared to the unaged specimens, we could rule out chemical aging as the cause of the increase. To distinguish between intrinsic strength changes and physical aging effects, the expected level of internal stresses was calculated according to Equation (13), by the following procedure.

The initial internal stress parameter K_0 (thermo-viscoelastic + aging), i.e. the internal stress level obtained after quenching, and not accounting for relaxation prior to and during the test, was obtained by integration over the temperature history. K_0 was therefore calculated from Equation (6) by accounting for the temperature dependence of β, as it is a function of E_m. The Young's modulus of the matrix E_m is temperature dependent, and was obtained from Equations (11) and (14). Since the internal stress parameter is a function of the geometry of the system, and particularly of the size of the droplet, an effective temperature ΔT_{eff} was obtained as shown in Figure 3, i.e. it was calculated from Equation (5) with E_m accounting for thermal history when $T_{test,1}$ is reached, and K_0 being known. The resulting temperature steps applied in the simulations are given in Table 4. Notice that this effective temperature does not

represent a stress free temperature, since the matrix stiffness is not a constant when re-heating the specimen. Rigorously, this effective temperature depends on the dimensions of the droplet. However, in this study, it was found that a deviation of less that 0.5% was involved in the range of droplet dimensions studied, so that it could be considered constant, and independent of the size of the system.

The last column of Table 4 deserves some further comments: when quenching the droplets, it was assumed, due to the small volume of the droplets, that an instantaneous cool-down takes place. This hypothesis results from a simplified evaluation of heat transfer over a microbond specimen in natural convection as discussed in the experimental section. Consequently, it was assumed that no aging occurs when the polymer is quenched from above T_g to room temperature, which resulted in the same ΔT_{eff} = -15°C for both the viscoelastic and the viscoelastic including aging cases. By contrast, a quench from 50°C to 37°C, followed by an isothermal aging time of 3 days at 37°C, and then a quench to room temperature, would involve different ΔT_{eff} if aging is accounted for or not. Aging slows down the relaxation process and therefore corresponds to an increase in ΔT_{eff} compared to viscoelastic behaviour.

Next, The microbond data were analysed using the various calculated values of K, and τ_0 was calculated for each value of τ_{exp} obtained. A unique τ_0 value was found, independent of aging time, and equal to 22.1±0.2 MPa. As a result, all the curves shown in Figure 11 have the same shear strength, and all variations are due to internal stresses. Therefore, aging properties of the interfacial region can be deduced from these of the bulk matrix only. Based upon this value of τ_0, it was also possible to calculate the values that would be obtained if the resin had a thermo-elastic or a viscoelastic behaviour. The two curves, indicated by dotted lines, are shown in Figure 11, and are respectively the lower and higher bounds to all possible experimental results. However, due to the viscoelastic nature of the resin, the lower bound is unattainable whatever the aging time. As a conclusion, for comparable thermal histories, it can be

stated that the experimental shear strength decreases upon aging, due to the slowing down of the relaxation of internal stresses.

The magnitude of the effect of internal stresses on practical adhesion is promoted to a great extent by the geometry of the system, particularly its small size, and is further explored in the following section. In a strength-based approach, the importance of correctly including internal stresses in the analysis is clearly demonstrated by the present results. If someone did the same experiments and neglected internal stresses, they would find values for τ_0 of 25.1 (unaged) and 37.6 MPa (aged) within a reasonable error (ca. 12% of standard deviation), and mistakenly conclude that physical aging increases the shear strength.

4.3 *Energy release rate formulation*

An alternate approach to analysis of microbond tests is the energy release rate or fracture mechanics results, which involves the energy necessary to propagate a crack at the interface, instead of the minimum stress needed to initiate a crack. To clarify the conclusions of the previous sections, the same microbond test results were analysed for interfacial toughness instead of for interfacial shear strength. This alternate analysis used Equation (18) to determine toughness from experimental shear stress. The required parameters are geometric and material properties of the fibre and matrix, the interfacial friction stress (τ_f), and the level of internal stresses characterised by an effective ΔT. The average friction stress was estimated from the experimental data after debonding (see Fig. 1). An alternate approach to find τ_f is to select the value that leads to minimum variations in observed toughness (on the grounds that toughness should be a geometry independent material property). This approach lead to a similar level of frictional stress and thus the experimental value was used.

To account for internal stresses, the experimental results were analysed with an effective ΔT. The level of internal stresses was calculated by using either a thermo-elastic analysis

or a full analysis that accounts for effects of relaxation of internal stresses and physical aging. The results for both unaged specimens (filled symbols) and aged specimens (open symbols) are given in Figure 12. When the internal stresses are calculated from a thermo-elastic analysis, the interfacial toughness of the unaged and aged specimens are both high and differ from each other by a factor of two. When the internal stresses are calculated properly, by accounting for all relaxations, the results for unaged and aged specimen drop considerable and become nearly equal. The average interfacial toughness for unaged specimens was $G_c = 262 \pm 14$ J/m^2 while the average interfacial toughness for aged specimens was $G_c = 266 \pm 10$ J/m^2.

An energy analysis therefore yields the same results as the previous strength analysis, which is that physical aging does not modify the intrinsic properties of the interface, rather, it modifies the relaxation rate of process-induced internal stresses. It is essential to note that in the analysis of the energy release rate, the internal stress contribution is of primary importance, since it represents the major part of the energy involved in the process [35]. If internal stresses were ignored, one would find a very low G_c of about 10 J/m^2 and probably draw erroneous conclusions about the true interfacial toughness properties. The important contribution of the friction factor was also demonstrated in reference [35], its major effect being to flatten the R-curves or to give a toughness that is independent of specimen geometry.

The energy analysis presents one advantage over the strength analysis. It can be noticed that the energy analysis involves more data points than were involved with the strength analysis. The reason is the energy analysis did not depend upon the loading point location, and results obtained for specimens which had slightly slipped between the Teflon jaws could still be used in the analysis. On the contrary, the strength analysis was very sensitive to this effect, and such data had to be discarded. The stability of the energy method is thought to be due to the approximation made in Equation (17) for calculating the microbond energy release rate.

Although this study only considered mode II failure of the interface, the results should also be of a broad significance for other failure modes, and therefore relevant for composite laminates.

5 CONCLUSIONS

Two methods for analysing the microbond test were presented; namely the interfacial shear strength and the interfacial toughness analyses. These methods were used for freshly cured and aged epoxy droplets on glass fibres, and were shown to yield similar results. For the model system chosen, no changes to the intrinsic mechanical properties of the interface were found upon structural recovery of the polymer matrix. This result was obtained providing that the relaxation of internal stresses, and the shift of relaxation times of the matrix when it was physically aged, was accounted for. This coupling between structural recovery and stress relaxation appeared to be critical in describing the behaviour of the model composite system considered, when both analyses were carried out.

6 ACKNOWLEDGEMENTS

The authors are indebted to the Swiss National Science Foundation for financial support. One author (J. A. Nairn) was supported by a grant from the Mechanics of Materials program at the National Science Foundation (CMS-9713356).

7 REFERENCES

1. Reifsnider, K.L., 1994. *Composites*, **25**(7): 461.
2. McKenna, G.B., 1994. *J. Res. NIST*, **99**(2): 169.
3. Kim, P., 1995. PhD Thesis. EPFL.
4. Struik, L.C.E., 1978. in *Physical Ageing in Amorphous Polymers and Other Materials*. Amsterdam: Elsevier Science Publishers.

5. Monaghan, M.R., L.C. Brinson, and R.D. Bradshaw, 1994. *Composites Engineering*, **4**: 1023.

6. Brinson, L.C. and T.S. Gates, 1995. *Int. J. Solids Structures*, **32**: 827.

7. Gurjar, A., D.G. Zollinger, and T. Tang, 1996. *Transp. Res. Rec.*, **1529**: 95.

8. Chambers, R.S., F.P. Gerstle, and S.L. Monroe, 1989. *J. Am. Ceram. Soc.*, **72**: 929.

9. Chiang, M.Y.M. and G.B. McKenna, 1994. *Polym. Eng. Sci.*, **34**: 1815.

10. Roy, S. and S. Denduluri, 1996. Proc. 1996 11th *Techn. Conf. of the Am. Soc. Compos*., Atlanta: Technomic Publ Co Inc, 603.

11. McKenna, G.B., Y. Leterrier, and C.R. Schultheisz, 1995. *Polym. Eng. Sci.*, **35**: 403.

12. Mendels, D.-A., Y. Leterrier and J.-A. E. Månson, 1999. Proc. *Duracosys'99*, Brussels: July 14-18, A.H. Cardon ed.

13. Zhandarov, S.F. and E.V. Pisanova, 1997. *Compos. Sci. Technol.*, **57**: 957.

14. Carroll, B.J., 1976. *J. Colloid Interf. Sci.*, **57**(3): p. 488.

15. Mendels, D.-A., Y. Leterrier, and J.-A.E. Månson, 1999. *J. Compos. Mater.*, **33**: p. 1525

16. Mendels, D.-A., Y. Leterrier, and J.-A.E. Månson, 2002. *J. Compos. Mater.,* in press

17. Zhandarov, S., E. Pisanova, E. Mäder, and J. A. Nairn, 2000. *J. Adhes. Sci. & Tech.*, **15**, p. 205

18. Page, S.A., L. Boogh, and J.-A. E Månson, 2002. *subm. to J. Appl. Polym. Sci*.

19. Gorbatkina, Y.A., 1992. in *Adhesive Strength in Fiber-Polymer Systems*. New York: Ellis Horwood.

20. Ferry, J.D., 1970. in *Viscoelastic Properties of Polymers*. New York: John Wiley and Sons.

21. Kohlrausch, F., 1847. *Pogg. Ann. Phys.*, **12**: 393.

22. Chow, T.S., 1985. *J. Non-Crystal. Sol.*, **75**: 209.

23. Ouali, N., M.B.M. Mangion, and J. Perez, 1993. *Phil. Mag. A*, **67**: 827.

24. Chow, T.S., 1990. *J. Mater. Sci.*, **25**: 957.

25. Kovacs, A.J., 1963. *Fortschr. Hochpolym.-Forsch.*, **3**: 394.

26. Lee, A. and G.B. McKenna, 1988. *Polymer*, **29**: 1812.

27. Lee, A. and G.B. McKenna, 1989. *Polymer*, **31**: 423.

28. McKenna, G.B., *et al.*, 1991. *J. Non-Cryst. Sol.*, **131-133**: 497.

29. G'sell, C. and G.B. McKenna, 1992. *Polymer*, **33**: 2103.

30. Moynihan, C.T., *et al.*, 1976. *Ann. N.Y. Acad. Sci.*, **279**: 15.

31. Narayanaswamy, O.S., 1971. *J. Am. Ceram. Soc.*, **54**: 491.

32. Williams, G. and D.C. Watts, 1970. *Trans. Faraday Soc.*, **66**: 80.

33. Chow, T.S., 1984. *Macromol.*, **17**: 2336.
34. Kovacs, A.J., *et al.*, 1979. *J. Polym. Sci., Polym. Phys. Ed.*, **17**: 1097.
35. Liu, C.-H. and J.A. Nairn, 1999. *Int. J. Adh. Adhes.*, **19**: 59.
36. Nairn, J.A., 2000. *Adv. Compos. Let.*, **9**: 373.
37. Crissman, J.M. and L.J. Zapas, 1989. *Polymer*, **30**:447.
38. Heisler, M.P., 1947. *Trans. ASME*, **69**:227.
39. Leendertz, J.A., 1970. *J. Phys. E.: Scientific Instruments*, **3**: 214.
40. Lin, K.S.C. and Aklonis, J.J., 1980. *J. Appl. Phys*., **51**:5125.
41. Smith, T.L., 1979. *J. Polym. Sci.: Polym. Phys. Ed*., **17**:2181.
42. Chow, T.S., 1988. *Polymer*, **29**: 1447.
43. Duran, R.S. and G.B. McKenna, 1990. *J. Rheol.*, **34**: 813.

8 LIST OF TABLES AND FIGURES

Table 1: Cooling and mounting times of the specimens

Specimen	t_{cool} (s)	*Range* °C	t_{test} (s)
rod	190	50 → 37	
	200	37 → 22	840
	220	50 → 22	840
microbond	<1s	50 → 37	
	<1s	37 → 22	180±5
	<1s	50 → 22	180±5

Table 2: Equation (11) parameters from relaxation experiments on epoxy aged at various times

aging time t_e (min)	E_0 (MPa)	E_∞ (MPa)	λ (s)
7	2210	201	46.8
127	2170	290	51.2
367	2330	302	66.7
727	2345	338	71.0
1447	2430	361	78.5
$2.59\ 10^5$	2745	551	107.8

Table 3: Parameters from aging experiments on the model epoxy network

Parameter	Value	Method	Refs.
α_l	$5.9\ 10^{-4}$ $cm^3/cm^3/K$	dilatometry	[43]
α_g	$2.0\ 10^{-4}$ $cm^3/cm^3/K$	dilatometry	[43]
T_g	42.1°C	DSC at 20°C/min	this work
	41.2°C	RSA at 20°C/min	-
Θ	$0.281\ K^{-1}$	RSA at 20°C/min	-
x	0.5	all aging experiments	This work, [26-28]
w	0.33±0.04	-	-

Table 4: Effective temperature steps applied in the calculation of the initial internal stress parameter K_0, in °C

	Thermo-elastic	Viscoelastic	Viscoelastic+aging
Quench from 50°C	30 (22.1)	15.5	15.5
Quench from 37°C	17	9.18	9.3

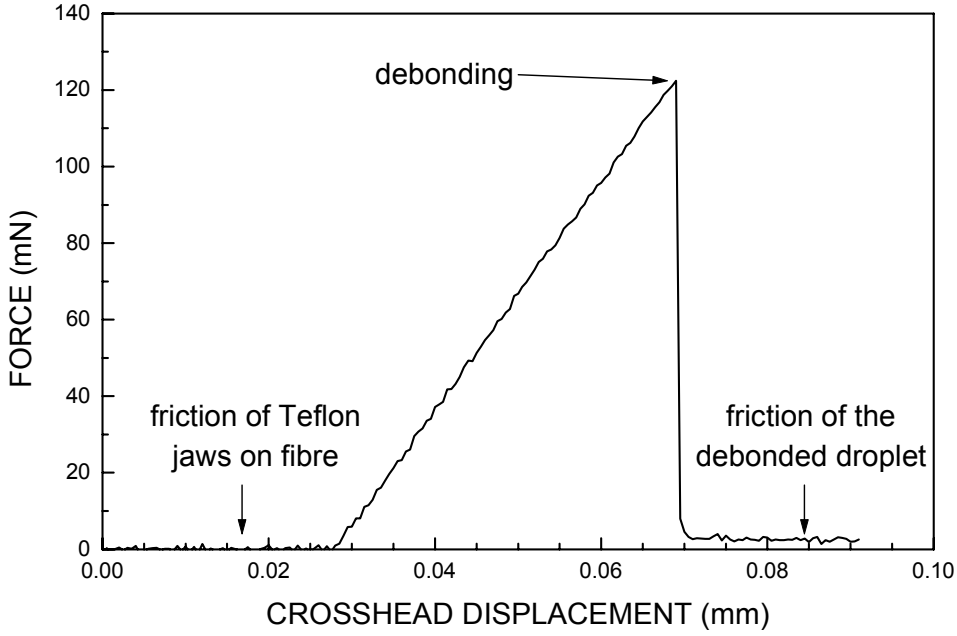
140
120
100
80
60
40
20
0
FORCE (mN)
debonding
friction of Teflon
jaws on fibre
friction of the
debonded droplet
0.00
0.02
0.04
0.06
0.08
0.10
CROSSHEAD DISPLACEMENT (mm)

Figure 1

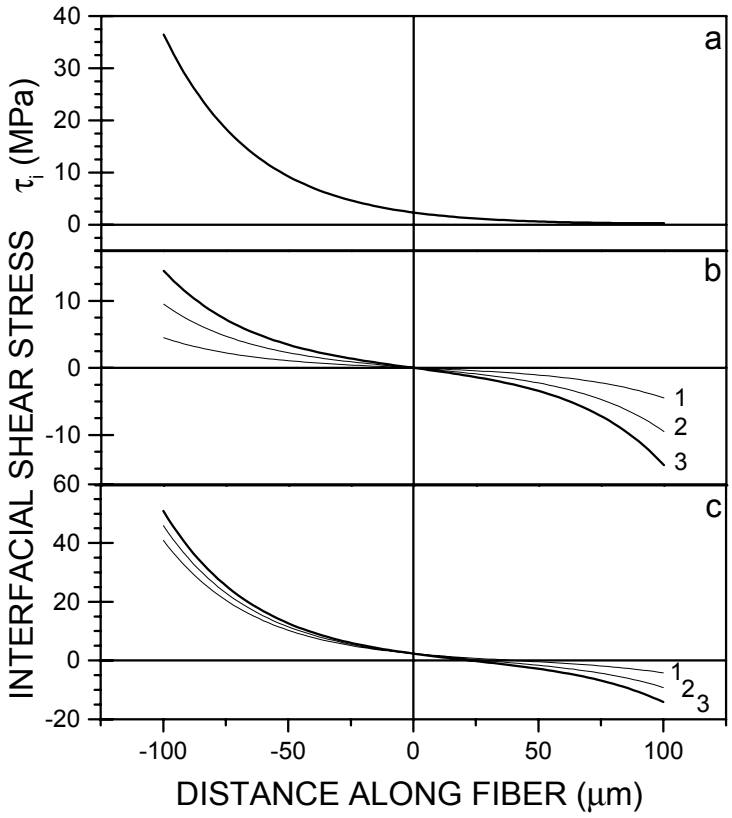
INTERFACIAL SHEAR STRESS τi (MPa)
DISTANCE ALONG FIBER (μm)
a
b
c
1
2
3
40
30
20
10
0
-10
60
-20
-100
-50
50
100

Figure 2

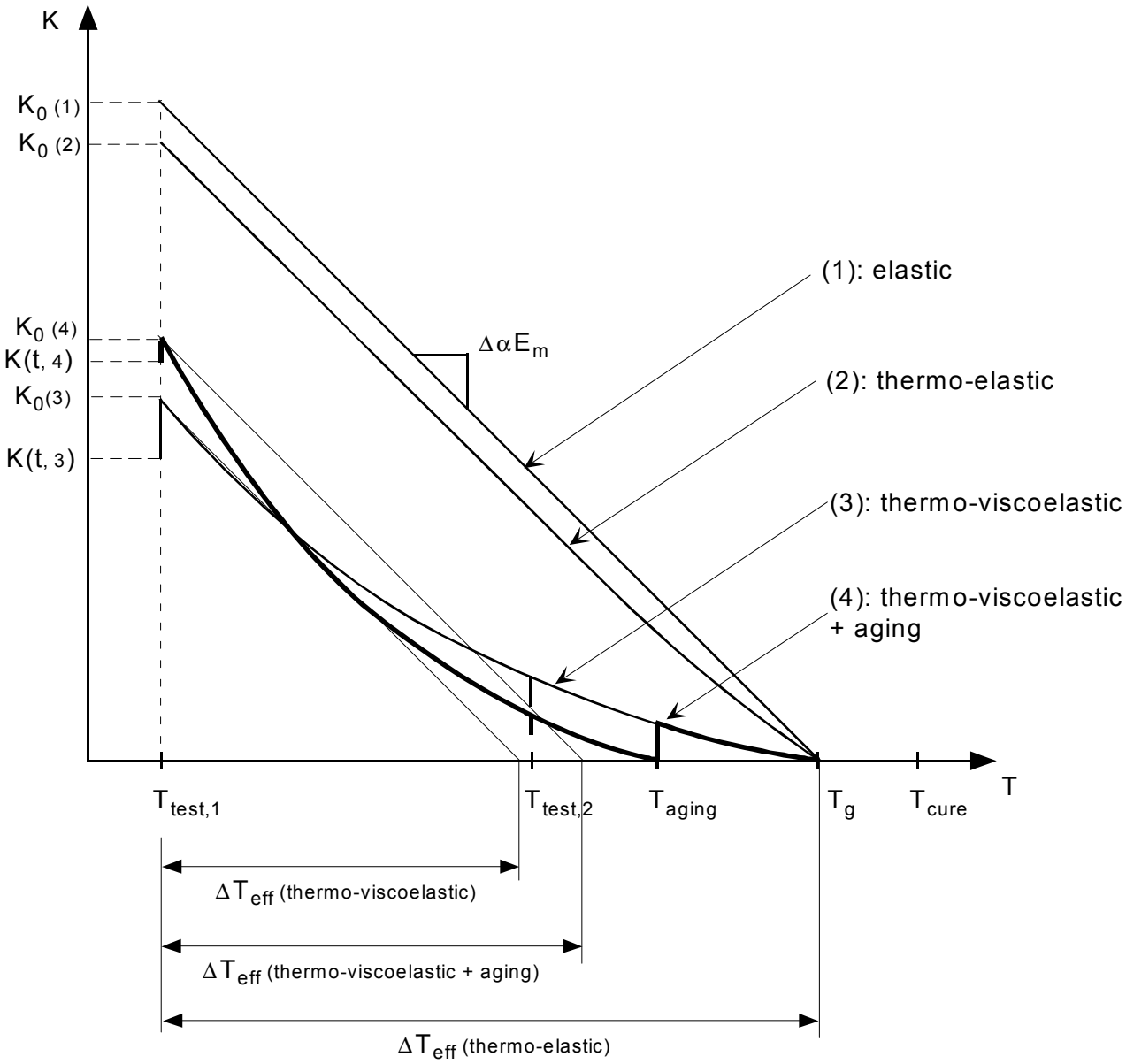
K
K0 (1)
K0 (2)
K0 (4)
K(t, 4)
K0(3)
K(t, 3)
(1): elastic
(2): thermo-elastic
(3): thermo-viscoelastic
(4): thermo-viscoelastic + aging
Δ α Em
T
Ttest,1
Ttest,2
Taging
Tg
Tcure
ΔTeff (thermo-viscoelastic)
ΔTeff (thermo-viscoelastic + aging)
ΔTeff (thermo-elastic)

Figure 3

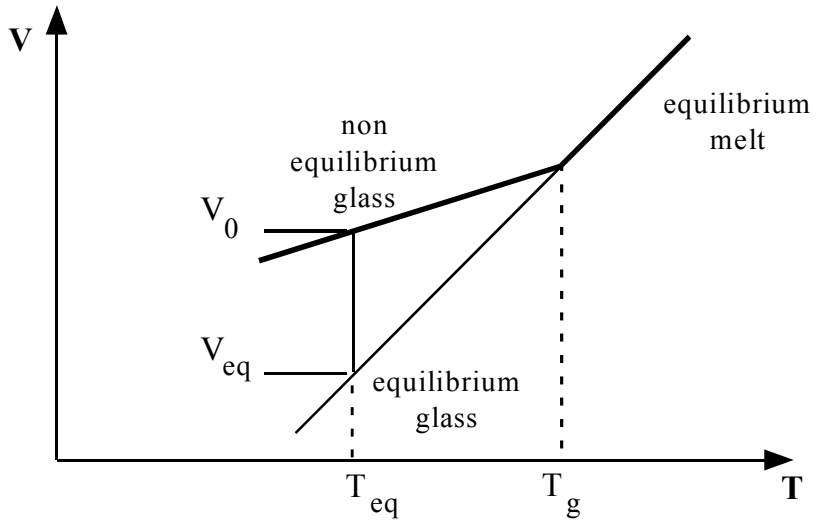
V
non
equilibrium
glass
equilibrium
melt
V0
Veq
equilibrium
glass
Teq
Tg
T

Figure 4

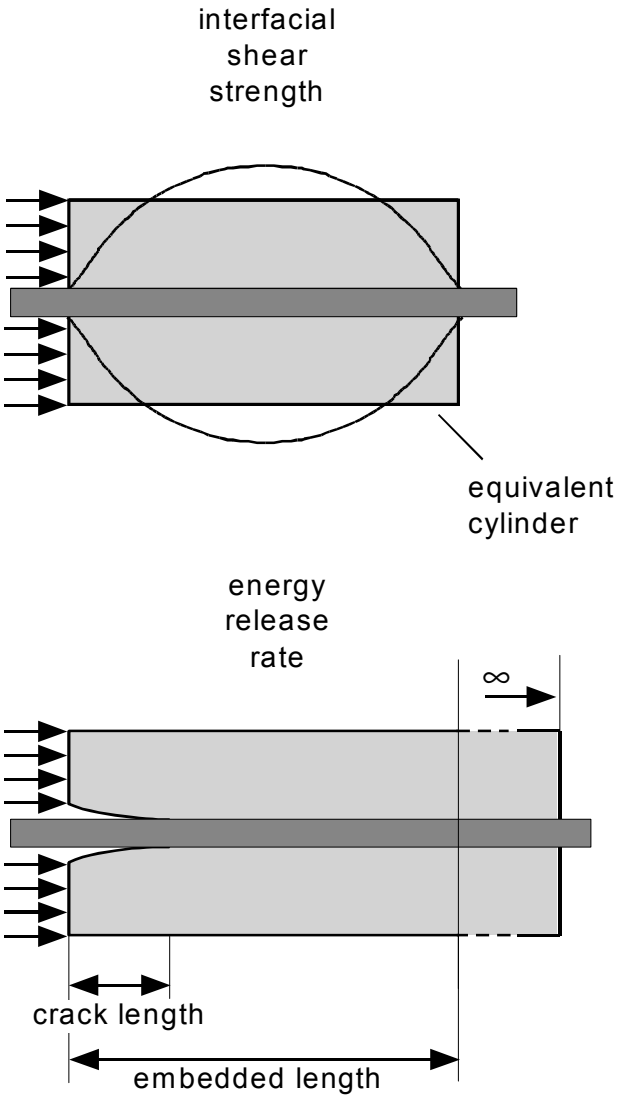
interfacial
shear
strength
equivalent
cylinder
energy
release
rate
∞
crack length
embedded length

Figure 5

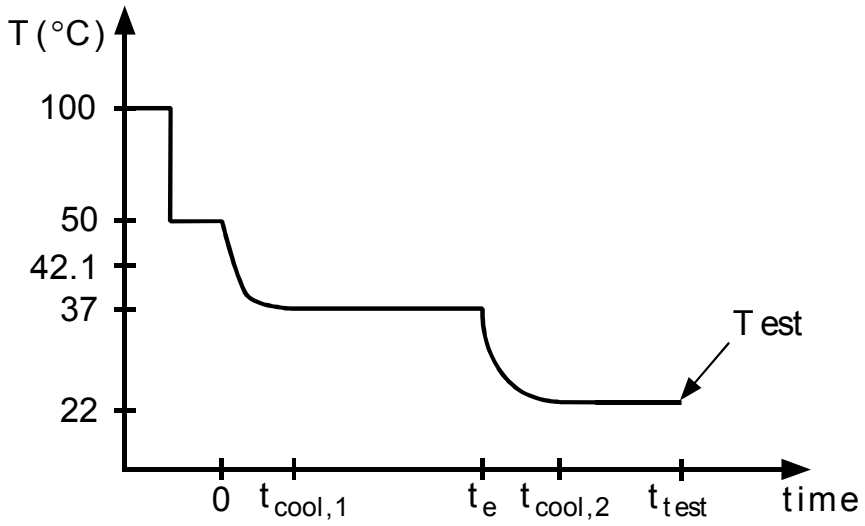

Figure 6

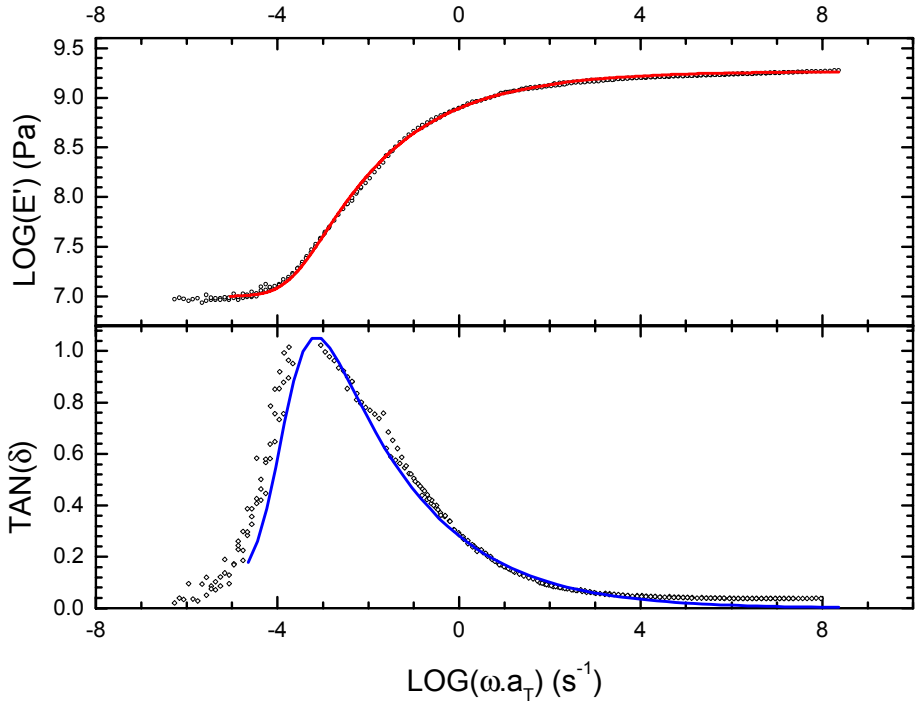

Figure 7

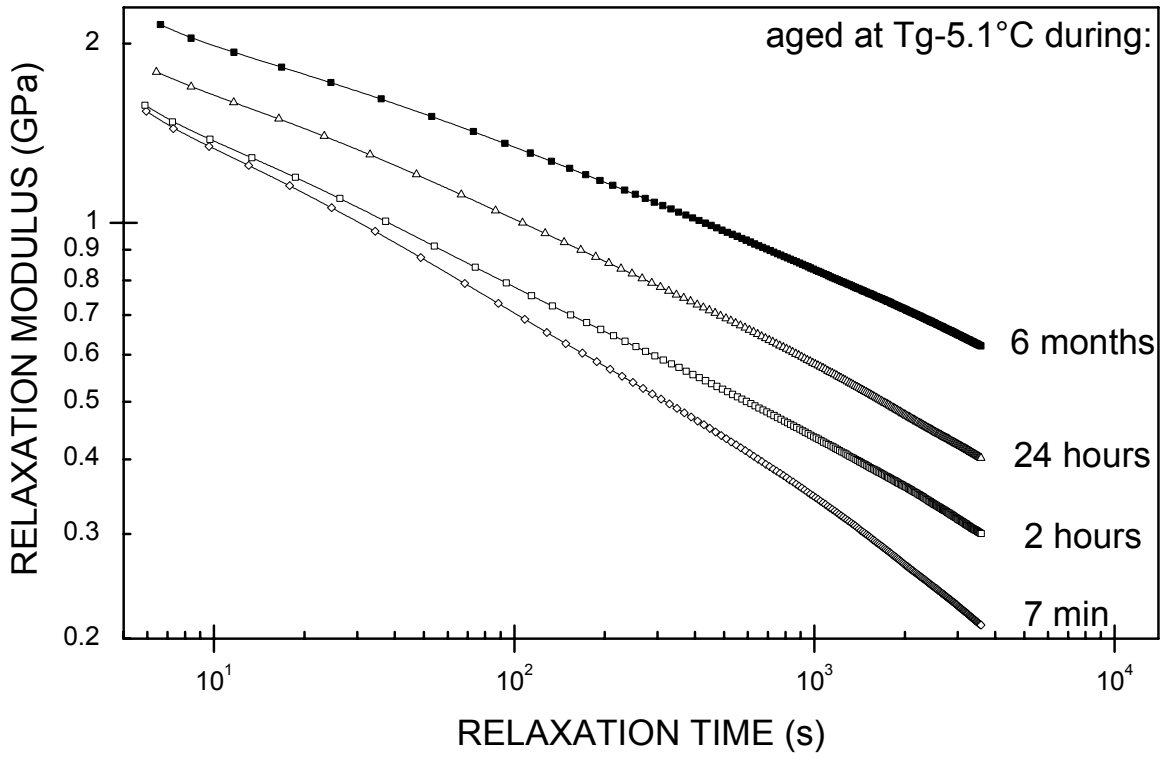
aged at Tg-5.1°C during:
6 months
24 hours
2 hours
7 min
RELAXATION MODULUS (GPa)
RELAXATION TIME (s)
2
1
0.9
0.8
0.7
0.6
0.5
0.4
0.3
0.2
10^1
10^2
10^3
10^4

Figure 8

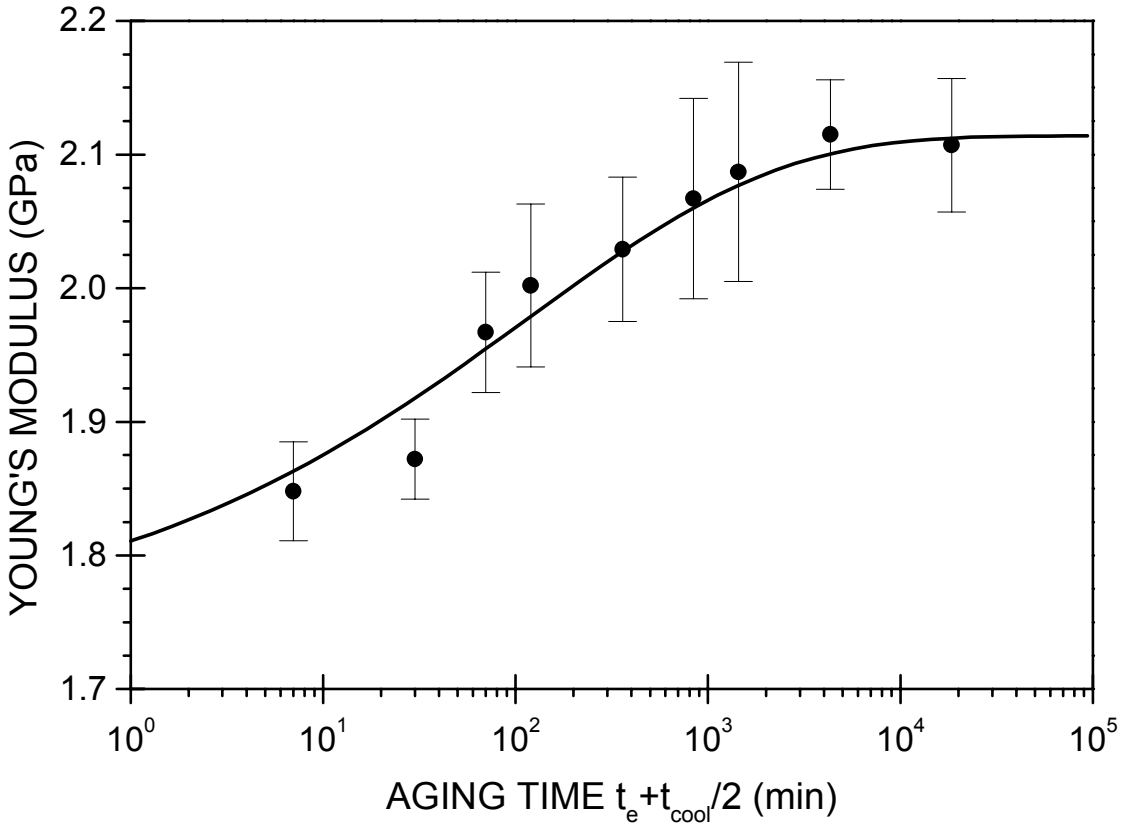
YOUNG'S MODULUS (GPa)
2.2
2.1
2.0
1.9
1.8
1.7
10^0
10^1
10^2
10^3
10^4
10^5
AGING TIME $t_e+t_{cool}/2$ (min)

Figure 9

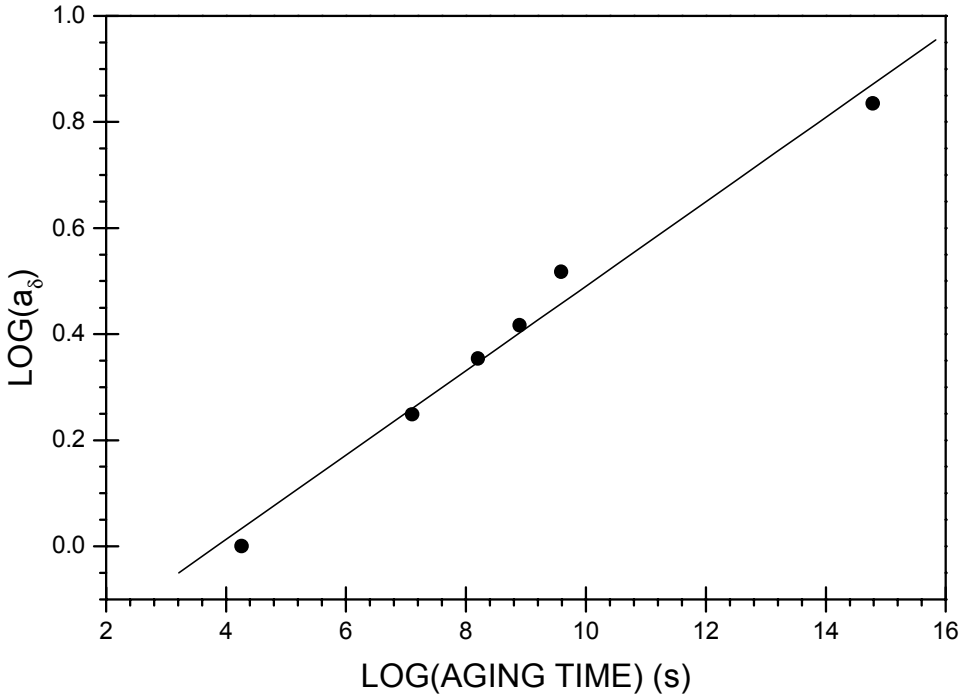

Figure 10

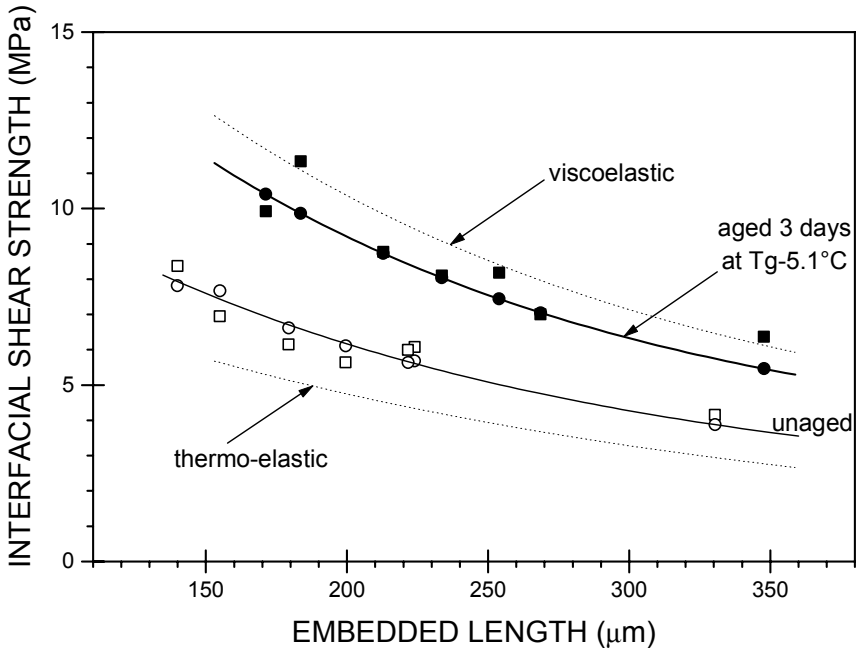
INTERFACIAL SHEAR STRENGTH (MPa)
EMBEDDED LENGTH (μm)
viscoelastic
aged 3 days
at Tg-5.1°C
unaged
thermo-elastic
0
5
10
15
150
200
250
300
350

Figure 11

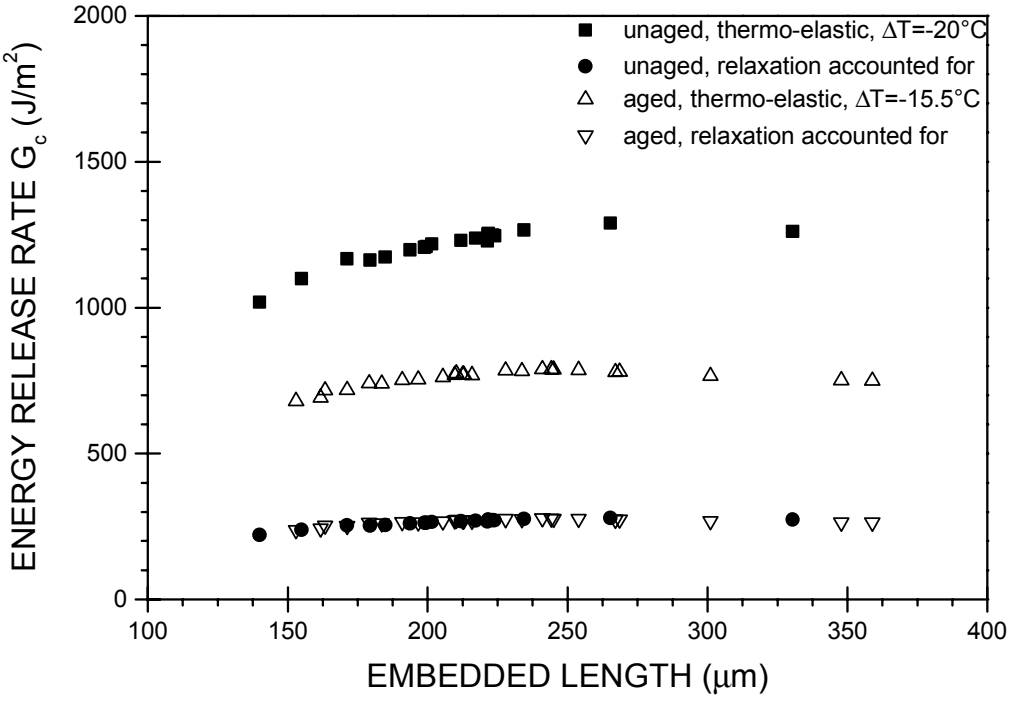
ENERGY RELEASE RATE G_c (J/m^2)
EMBEDDED LENGTH (μm)
unaged, thermo-elastic, ΔT=-20°C
unaged, relaxation accounted for
aged, thermo-elastic, ΔT=-15.5°C
aged, relaxation accounted for
2000
1500
1000
500
0
100
150
200
250
300
350
400

Figure 12